number of corpora lutea has not been reported so far for the other PFAAs (ATSDR, 2009; Luebker *et al.,* 2005a). Ovarian follicle development is known to be regulated by the hypothalamic-pituitary-ovarian axis; however, the present result that no effects were found on estrous cyclicity, on the copulation, fertility or delivery index, or on the weight and histopathology of male and female reproductive and endocrine organs denies the possibility that PFOdA affected the axis. Since the recent studies indicate that many other intra-ovarian signaling cascades affect follicular development (Richards and Pangas, 2010), PFOdA might act on such cascades.

PFOdA administration slightly decreased the delivery, live birth and viability index at 1,000 mg/kg/day, and the values were outside the normal range for this strain of rat in the laboratory that performed this study (historical control range for the last twelve years: 84.5-97.0%, 97.7-100.0% and 96.2-100%, respectively). Further, the birth weight of pups was decreased and postnatal body weight gain was inhibited at 1,000 mg/kg/day. Such effects on prenatal and postnatal development could be attributed to secondary effects due to maternal toxicity such as inhibition of body weight gain, but the lipophilic property of PFOdA also indicates the possibility that it was transferred via placenta and/or breast milk and affected the fetuses/pups directly. Previous studies demonstrated developmental effects of the other PFAAs, which were observed even at doses which produced no maternal toxicity (ATSDR, 2009; Butenhoff *et al.,* 2004; Case *et al.,* 2001; Das *et al.,* 2008; Harris and Birnbaum, 1989; Lau *et al.,* 2006, 2003; Luebker *et al.,* 2005a, 2005b; Thibodeaux *et al.,* 2003). Abbott *et al.* (2007) reported an increase in the incidence of full litter loss, reduction of neonatal survival and body weight gain and delayed eye opening in mice given PFOA during days 1-17 of gestation at 0.6 mg/kg/day and above. Interestingly, such developmental effects were not detected in PPARα knockout mice given the same dose. Investigating the PPARα agonistic activity of PFOdA might provide useful information to understand the mechanism of the developmental effects as well as hepatotoxicity.

In summary, oral gavage administration of PFOdA primarily affected the liver, causing centrilobular hepatocyte hypertrophy and necrosis. Other effects included inhibition of body weight gain, anemia, prolongation of APTT and decreased pancreatic zymogen granules. These toxic effects observed at the end of the 42- to 56-day administration period were also detected after the 14-day recovery period. PFOdA also showed reproductive/developmental toxicity: the number of corpora lutea and implantation, total number of pups born, the number of live pups and birth weight of pups were decreased, and the postnatal body weight gain was inhibited. Based on these findings, the NOAEL of PFOdA was considered to be 40 mg/kg/day for repeated dose toxicity and 200 mg/kg/day for reproductive/developmental toxicity.

ACKNOWLEDGMENTS

This study was undertaken under the Japanese safety programmes for existing chemicals funded by the Ministry of Health, Labour and Welfare, Japan, and supported by a Health and Labour Sciences Research Grant (H22-Kenki-Ippan-006) from the Ministry of Health, Labour and Welfare, Japan.

REFERENCES

3M (year not specified): Information about PFOS and PFOA. Available at: http://solutions.3m.com/wps/portal/3M/en_US/PFOS/PFOA. Accessed on July 15, 2011.

Abbott, B.D., Wolf, C.J., Schmid, J.E., Das, K.P., Zehr, R.D., Helfant, L., Nakayama, S., Lindstrom, A.B., Strynar, M.J. and Lau, C. (2007): Perfluorooctanoic acid induced developmental toxicity in the mouse is dependent on expression of peroxisome proliferator activated receptor-alpha. Toxicol. Sci., **98**, 571-581.

ATSDR (2009): Toxicological Profile for Perfluoroalkyls (Draft for Public Comment), US Department of health and human services, Public health service, Agency for Toxic Substances and Disease Registry (ATSDR). Available at: http://www.atsdr.cdc.gov/toxprofiles/tp.asp?id=1117&tid=237. Accessed on July 19, 2011.

Butenhoff, J.L., Kennedy, G.L.Jr., Frame, S.R., O'Connor, J.C. and York, R.G. (2004): The reproductive toxicology of ammonium perfluorooctanoate (APFO) in the rat. Toxicology, **196**, 95-116.

Canada, E. (2010): Perfluorooctane sulfonate (PFOS), its salts and its precursors. Available at: http://www.ec.gc.ca/toxiques-toxics/Default.asp?lang=En&n=98E80CC6-1&xml=ECD5A576-CEE5-49C7-B26A-88007131860D. Accessed on July 15, 2011.

Case, M.T., York, R.G. and Christian, M.S. (2001): Rat and rabbit oral developmental toxicology studies with two perfluorinated compounds. Int. J. Toxicol., **20**, 101-109.

Chang, S.C., Das, K., Ehresman, D.J., Ellefson, M.E., Gorman, G.S., Hart, J.A., Noker, P.E., Tan, Y.M., Lieder, P.H., Lau, C., Olsen, G.W. and Butenhoff, J.L. (2008): Comparative pharmacokinetics of perfluorobutyrate in rats, mice, monkeys, and humans and relevance to human exposure via drinking water. Toxicol. Sci., **104**, 40-53.

Chengelis, C.P., Kirkpatrick, J.B., Radovsky, A. and Shinohara, M. (2009): A 90-day repeated dose oral (gavage) toxicity study of perfluorohexanoic acid (PFHxA) in rats (with functional observational battery and motor activity determinations). Reprod. Toxicol., **27**, 342-351.

Das, K.P., Grey, B.E., Zehr, R.D., Wood, C.R., Butenhoff, J.L., Chang, S.C., Ehresman, D.J., Tan, Y.M. and Lau, C. (2008): Effects of perfluorobutyrate exposure during pregnancy in the mouse. Toxicol. Sci., **105**, 173-181.

EU (2006): Directive 2006/122/ECOF. The European Parliament and of the Council of 12 December 2006, amending for the 30th time Council Directive 76/769/EEC on the approximation of the

laws, regulations and administrative provisions of the Member States relating to restrictions on the marketing and use of certain dangerous substances and preparations (perfluorooctane sulfonates). Official Journal of the European Union (EU). Available at: http://eur-lex.europa.eu/LexUriServ/LexUriServ.do?uri=OJ:L:2006:372:0032:0034:en:PDF. Accessed on July 15, 2011.

Fang, X., Zhang, L., Feng, Y., Zhao, Y. and Dai, J. (2008): Immunotoxic effects of perfluorononanoic acid on BALB/c mice. Toxicol. Sci., **105**, 312-321.

Goldenthal, E.I. (1978): Final report: Ninety day subacute rat toxicity study on Fluorad® Fluorochemical FC-143. International Research and Development Corporation. Study No. 137-089. 3M Reference No. T-3141. US EPA AR226-0441, cited in US EPA (2005).

Goldenthal, E.I., Jessup, D.C., Geil, R.G., Jefferson, N.D. and Arceo, R.J. (1978): Ninety-day subacute rat study. Study No. 137-085. International Research and Development Corporation, cited in OECD (2002).

Griffith, F.D. and Long, J.E. (1980): Animal toxicity studies with ammonium perfluorooctanoate. Am. Ind. Hyg. Assoc. J., **41**, 576-583.

Harris, M.W. and Birnbaum, L.S. (1989): Developmental toxicity of perfluorodecanoic acid in C57BL/6N mice. Fundam. Appl. Toxicol., **12**, 442-448.

Hekster, F.M., Laane, R.W. and de Voogt, P. (2003): Environmental and toxicity effects of perfluoroalkylated substances. Rev. Environ. Contam. Toxicol., **179**, 99-121.

Ioannidis, O., Lavrentieva, A. and Botsios, D. (2008): Nutrition support in acute pancreatitis. JOP, **9**, 375-390.

Japanese Animal Welfare Law (2005): Act on Welfare and Management of Animals. Act No. 105 of October 1, 1973. As amended up to Act No. 68 of June 22, 2005.

Kawashima, Y., Kobayashi, H., Miura, H. and Kozuka, H. (1995): Characterization of hepatic responses of rat to administration of perfluorooctanoic and perfluorodecanoic acids at low levels. Toxicology, **99**, 169-178.

Kemper, R.A. (2003): Perfluorooctanoic acid: toxicokinetics in the rat. Association of plastics manufactures of Europe. Submitted to the US EPA's admistrative record. AR226-1499, cited in ASTDR (2009).

Kennedy, G.L.Jr. (1987): Increase in mouse liver weight following feeding of ammonium perfluorooctanoate and related fluorochemicals. Toxicol. Lett., **39**, 295-300.

Kudo, N., Bandai, N., Suzuki, E., Katakura, M. and Kawashima, Y. (2000): Induction by perfluorinated fatty acids with different carbon chain length of peroxisomal beta-oxidation in the liver of rats. Chem. Biol. Interact., **124**, 119-132.

Kudo, N., Katakura, M., Sato, Y. and Kawashima, Y. (2002): Sex hormone-regulated renal transport of perfluorooctanoic acid. Chem. Biol. Interact., **139**, 301-316.

Kudo, N., Suzuki-Nakajima, E., Mitsumoto, A. and Kawashima, Y. (2006): Responses of the liver to perfluorinated fatty acids with different carbon chain length in male and female mice:in relation to induction of hepatomegaly, peroxisomal beta-oxidation and microsomal 1-acylglycerophosphocholine acyltransferase. Biol. Pharm. Bull., **29**, 1952-1957.

Lau, C., Anitole, K., Hodes, C., Lai, D., Pfahles-Hutchens, A. and Seed, J. (2007): Perfluoroalkyl acids: a review of monitoring and toxicological findings. Toxicol. Sci., **99**, 366-394.

Lau, C., Thibodeaux, J.R., Hanson, R.G., Narotsky, M.G., Rogers, J.M., Lindstrom, A.B. and Strynar, M.J. (2006): Effects of perfluorooctanoic acid exposure during pregnancy in the mouse. Toxicol. Sci., **90**, 510-518.

Lau, C., Thibodeaux, J.R., Hanson, R.G., Rogers, J.M., Grey, B.E., Stanton, M.E., Butenhoff, J.L. and Stevenson, L.A. (2003): Exposure to perfluorooctane sulfonate during pregnancy in rat and mouse. II: postnatal evaluation. Toxicol. Sci., **74**, 382-392.

Lieder, P.H., Chang, S.C., York, R.G. and Butenhoff, J.L. (2009a): Toxicological evaluation of potassium perfluorobutanesulfonate in a 90-day oral gavage study with Sprague-Dawley rats. Toxicology, **255**, 45-52.

Lieder, P.H., York, R.G., Hakes, D.C., Chang, S.C. and Butenhoff, J.L. (2009b): A two-generation oral gavage reproduction study with potassium perfluorobutanesulfonate (K+PFBS) in Sprague Dawley rats. Toxicology, **259**, 33-45.

Luebker, D.J., Case, M.T., York, R.G., Moore, J.A., Hansen, K.J. and Butenhoff, J.L. (2005a): Two-generation reproduction and cross-foster studies of perfluorooctanesulfonate (PFOS) in rats. Toxicology, **215**, 126-148.

Luebker, D.J., York, R.G., Hansen, K.J., Moore, J.A. and Butenhoff, J.L. (2005b): Neonatal mortality from in utero exposure to perfluorooctanesulfonate (PFOS) in Sprague-Dawley rats: dose-response, and biochemical and pharamacokinetic parameters. Toxicology, **215**, 149-169.

Martin, J.W., Mabury, S.A., Solomon, K.R. and Muir, D.C. (2003): Bioconcentration and tissue distribution of perfluorinated acids in rainbow trout (Oncorhynchus mykiss). Environ. Toxicol. Chem., **22**, 196-204.

ME (2006): Standards Relating to the Care, Management of Laboratory Animals and Relief of Pain. Announcement No. 88 of Ministry of the Environment (ME), Japan, dated April 28, 2006.

ME (2008) 19. Perfluorooctane sulfonic acid and its salt forms (Perfluorooctane sulfonate: PFOS, in Japanese). Initial environmental risk assessment of chemicals, Vol.6, Ministry of the Environment (ME). Available at: http://www.env.go.jp/chemi/report/h19-03/pdf/chpt1/1-2-2-19.pdf. Accesed on July 27, 2011.

ME, METI and MHLW (2008): Standard concerning testing laboratories implementing tests for new chemical substances etc.. Joint notification by director generals of Environmental Policy Bureau, Ministry of the Environment (ME), Japan (Kanpokihatsu No. 031121004) and Manufacturing Industries Bureau, Ministry of Economy, Trade and Industry (METI), Japan (Seikyokuhatsu No. 3), dated November 17, 2003 and by director general of Pharmaceutical and Food Safety Bureau, Ministry of Health, Labour and Welfare (MHLW), Japan (Yakusyokuhatsu No. 1121003), dated November 21, 2003. As amended up to July 4, 2008.

Mertens, J.J., Sved, D.W., Marit, G.B., Myers, N.R., Stetson, P.L., Murphy, S.R., Schmit, B., Shinohara, M. and Farr, C.H. (2010): Subchronic toxicity of S-111-S-WB in Sprague Dawley rats. Int. J. Toxicol., **29**, 358-371.

MHLW, ME and NITE (year not specified): Japan CHEmicals Collaborative Knowledge database (J-CHECK, in Japanese). Ministry of Health, Labour and Welfare (MHLW), Ministry of the Environment (ME) and National Institute of Technology and Evaluation (NITE), Japan. Available at: http://www.safe.nite.go.jp/jcheck/Top.do;jsessionid=70E9B212CA59B38B6F8FC6B4BF47FEDD. Accessed on July 15, 2011.

OECD (1996): Organisation for Economic Co-operation and Development (OECD) Guidelines for the Testing of Chemicals, Section 4: Health Effects, Test No. 422: Combined Repeated Dose Toxicity Study with the Reproduction/Developmental Toxicity Screening Test. Adopted on 22 March, 1996.

OECD (2002): Hazard assessment of perfluorooctane sulfonate

(PFOS) and its salts. Organisation for Economic Co-operation and Development (OECD). ENV/JM/RD(2002)17/FINAL. Available at: http://www.oecd.org/dataoecd/23/18/2382880.pdf. Accessed on July 15, 2011. .

OECD (2007): Report of an OECD workshop on perfluorocarbosylic acids (PFCAs) and precursors. Organisation for Economic Co-operation and Development (OECD), Environment directorate, Joint meeting of the chemicals committee and the working party on chemicals, pesticides and biotechnology. Available at: http://www.oecd.org/officialdocuments/displaydocumentpdf/?cote=env/jm/mono(2007)11&doclanguage=en. Accessed on Juny 15, 2011.

Ohmori, K., Kudo, N., Katayama, K. and Kawashima, Y. (2003): Comparison of the toxicokinetics between perfluorocarboxylic acids with different carbon chain length. Toxicology, **184**, 135-140.

Ove, P., Coetzee, M.L., Chen, J. and Morris, H.P. (1972): Differences in synthesis and degradation of serum proteins in normal and hepatoma-bearing animals. Cancer Res., **32**, 2510-2518.

Perkins, R.G., Butenhoff, J.L., Kennedy, G.L.Jr. and Palazzolo, M.J. (2004): 13-week dietary toxicity study of ammonium perfluorooctanoate (APFO) in male rats. Drug Chem. Toxicol., **27**, 361-378.

Permadi, H., Lundgren, B., Andersson, K. and DePierre, J.W. (1992): Effects of perfluoro fatty acids on xenobiotic-metabolizing enzymes, enzymes which detoxify reactive forms of oxygen and lipid peroxidation in mouse liver. Biochem. Pharmacol., **44**, 1183-1191.

Permadi, H., Lundgren, B., Andersson, K., Sundberg, C. and DePierre, J.W. (1993): Effects of perfluoro fatty acids on peroxisome proliferation and mitochondrial size in mouse liver: dose and time factors and effect of chain length. Xenobiotica, **23**, 761-770.

Richards, J.S. and Pangas, S.A. (2010) The ovary: basic biology and clinical implications. J. Clin. Invest., **120**, 963-972.

Schultz, M.M., Barofsky, D.F. and Field, J.A. (2003): Fluorinated Alkyl Surfactants. Environ. Eng. Sci., **20**, 487-501.

Shi, Z., Zhang, H., Liu, Y., Xu, M. and Dai, J. (2007): Alterations in gene expression and testosterone synthesis in the testes of male rats exposed to perfluorododecanoic acid. Toxicol. Sci., **98**, 206-215.

Sibinski, L.J. (1987): Final report of a two year oral (diet) toxicity and carcinogenicity study of fluorochemical FC-143 (perfluorooctanane ammonium carboxylate) in rats. Vol.1-4, 3M Company/RIKER Exp. No.0281CR0012; 8EHQ-1087-0394, cited in US EPA (2005).

Stockholm Convention (2010): The 9 new POPs under the Stockholm Convention. Stockholm Convention on Persistent Organic Pollutants (POPs). Available at: http://chm.pops.int/Programmes/New%20POPs/The%209%20new%20POPs/tabid/672/language/en-GB/Default.aspx. Accessed on July 15, 2011.

Stump, D.G., Holson, J.F., Murphy, S.R., Farr, C.H., Schmit, B. and Shinohara, M. (2008): An oral two-generation reproductive toxicity study of S-111-S-WB in rats. Reprod. Toxicol., **25**, 7-20.

Thibodeaux, J.R., Hanson, R.G., Rogers, J.M., Grey, B.E., Barbee, B.D., Richards, J.H., Butenhoff, J.L., Stevenson, L.A. and Lau, C. (2003): Exposure to perfluorooctane sulfonate during pregnancy in rat and mouse. I: maternal and prenatal evaluations. Toxicol. Sci., **74**, 369-381.

Thomford, P.J. (2002): Final report: 104-seek dietary chronic toxicity and carcinogenicity study with perfluorooctane sulfonic acid potassium salt (PFOS; T-6295) in rats. Covance study No. 6329-183, Covence Laboratories Inc. US EPA AR226-1070a, AR226-0956, cited in OECD (2002) and ME (2008).

US EPA (2000): EPA and 3M Announce Phase Out of PFOS. News Release By Date. United States Environmental Protection Agency (US EPA). May 16 2000. Available at: http://yosemite.epa.gov/opa/admpress.nsf/0/33aa946e6cb11f35852568e1005246b4?opendocument. Accessed on July 15, 2011.

US EPA (2005): Draft risk assessment of the potential human health effects associated with exposure to perfluorooctanoic acid and its salts. United States Environmental Protection Agency (EPA), Office of Pollution Prevention and Toxics, Risk Assessment Division. Available at: http://www.epa.gov/oppt/pfoa/pubs/pfoarisk.pdf. Accessed on July 19, 2011.

US EPA (2008a): Perfluorooctanoic acid (PFOA) and fluorinated telomers. United States Environmental Protection Agency (US EPA). Available at: http://www.epa.gov/oppt/pfoa/. Accessed on July 15, 2011. .

US EPA (2008b): Significant new uses of chemical substances. United States Environmental Protection Agency (US EPA). Code of Federal Regulations. 40 CFR 721. Available at: http://www.gpo.gov/fdsys/pkg/CFR-2008-title40-vol30/pdf/CFR-2008-title40-vol30-part721.pdf. Accessed on July 15, 2011. .

van Otterdijk, F.M. (2007a): Repeated dose 28-day oral toxicity study with MTDID-8391 by daily gavage in the rat, followed by a 21-day recovery. NOTOX Project 470677. Available at: http://www.health.state.mn.us/divs/eh/hazardous/28daymaintext.pdf. Accessed on July 19, 2011.

van Otterdijk, F.M. (2007b): Repeated dose 90-day oral toxicity study with MTDID 8391 by daily gavage in the rat, followed by a 3-week recovery, NOTOX Project 484492. Available at http://www.health.state.mn.us/divs/eh/hazardous/90daypfbareport.pdf. Accessed on July 19, 2011.

Xie, Y., Yang, Q., Nelson, B.D. and DePierre, J.W. (2003): The relationship between liver peroxisome proliferation and adipose tissue atrophy induced by peroxisome proliferator exposure and withdrawal in mice. Biochem. Pharmacol., **66**, 749-756.

Yang, Q., Xie, Y., Alexson, S.E., Nelson, B.D. and DePierre, J.W. (2002): Involvement of the peroxisome proliferator-activated receptor alpha in the immunomodulation caused by peroxisome proliferators in mice. Biochem. Pharmacol., **63**, 1893-1900.

Yang, Q., Xie, Y. and Depierre, J.W. (2000): Effects of peroxisome proliferators on the thymus and spleen of mice. Clin. Exp. Immunol., **122**, 219-226.

Zhang, H., Shi, Z., Liu, Y., Wei, Y. and Dai, J. (2008): Lipid homeostasis and oxidative stress in the liver of male rats exposed to perfluorododecanoic acid. Toxicol. Appl. Pharmacol., **227**, 16-25.

Alternative Approach to Estimate the Allocations to Drinking-water of THMs and HAAs

Dawei Quan*, Ryosuke Okashita**, Teruo Muto***, Yasuo Yanagibashi****, Shinya Echigo*****, Sadahiko Itoh*****, Yumiko Ohkouchi*****, Hideto Jinno******

*Graduate School of Engineering, Kyoto University, Nishikyoku, Kyoto, 615-8540, Japan
(E-mail: *davidquan@urban.env.kyoto-u.ac.jp*)
**West Japan Railway Company, Kitaku, Osaka, 530-8341, Japan
(E-mail: *ryo_ambition@yahoo.co.jp*)
*** Metawater Company Limited, Mizuhoku, Nagoya, 467-8530, Japan
(E-mail: *muto@metawater.co.jp*)
****Fukuoka Women's University, Higashiku, Fukuoka, 813-8529, Japan
(E-mail: *yanagibashi@fwu.ac.jp*)
*****Graduate School of Global Environmental Studies, Kyoto University, Nishikyoku, Kyoto, 615-8540, Japan
(E-mail: *Echigo@urban.env.kyoto-u.ac.jp; itoh@urban.env.kyoto-u.ac.jp; yohkouchi@urban.env.kyoto-u.ac.jp*)
******National Institute of Health Sciences, Setagayaku, Tokyo, 158-8501, Japan
(E-mail: *jinno@nihs.go.jp*)

Abstract
The allocation-to-drinking-water of trihalomethanes (THMs) and Haloacetic acids (HAAs) were intensively estimated as background data set for a more rationally establishment of standard value of drinking water. The ingestion exposure via drinking water were separately considered as via direct tap water intake and via indirect tap water intake (as cooking matrix) through investigating the THM and HAA concentrations in tap-water-prepared and reagent-water-prepared dietary samples. The results showed that preparation with tap water leads to generally higher THM and HAA concentrations and ingestion exposure amounts. Therefore, it is necessary to consider the ingestion exposure separately when estimate the allocation factors of THMs and HAAs.

Keywords
THMs; HAAs; drinking water; ingestion exposure; allocation factor

BACKGROUND

As two major disinfection byproducts (DBPs) of drinking water, trihalomethanes (THMs) and haloacetic acids (HAAs) have attracted extensive attention because of their carcinogenic potencies in mammals (Clark *et al.*, 1992). In the current Drinking-water Quality Standards of Japan, it is considered appropriate to use the tolerable daily intake (TDI) approach to derive the standard values for four and two species of THMs and HAAs as shown in Equation 1 and Table 1. In this approach, a daily water consumption of 2 Litres by a person weighing 50 kg is generally assumed (Ministry of Health, Labor and Welfare, Japan, 2009). The allocation-to-drinking-water (hereinafter, abbreviated as allocation factor) is also an important part of the derivation. It represents the fraction of the ingestion exposure via tap water intake in the total exposure via all exposure routes (dietary ingestion, inhalation and transdermal as shown in situation (a) of Figure 1. And because the information related to the multi-route exposure of them is rather limited, a factor of 20% is temporarily applied.

However, the daily water consumption of tap water could be considered as the summation of daily direct tap water intake and indirect tap water intake as cooking matrix. And in the same way, their ingestion exposure should also be estimated separately as shown in situation (b) of Figure 1. Following this consideration, this research is designed to seek for a more precise establishment of allocation factor, and focuses on the difference of direct and indirect ingestion exposure via tap water intake.

$$\text{Standard value (mg/L)} = \frac{\text{TDI } (\mu g/(kg \cdot day)) \times \text{body weight (kg)} \times \text{allocation factor (-)}}{\text{Daily water consumption (L)} \times 1000} \quad \text{Eq. (1)}$$

Table 1. Regulatory frameworks of THMs and HAAs in Japan

	TDI (μg/(kg·day))	Daily water consumption (L/day)	Body weight (kg)	Allocation factor (-)	Standard value (mg/L)
Chloroform (TCM)	12.9	2	50	20%	0.06
Bromodichloromethane (BDCM)	6.1	2	50	20%	0.03
Dibromochloromethane (DBCM)	21	2	50	20%	0.1
Tribromomethane (TBM)	17.9	2	50	20%	0.09
Monochloroacetic acid (MCA)	3.5	2	50	20%	0.02
Trichloroacetic acid (TCA)	32.5	2	50	20%	0.2

[b] Ministry of Health, Labor and Welfare, Japan (2008)

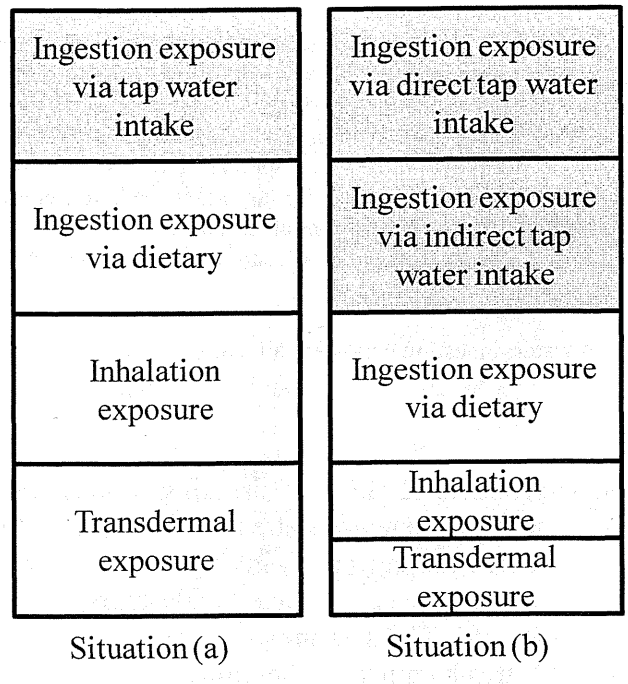

Figure 1. Conceptual illustration of the allocation-to-drinking-water (grey portion)

METHODOLOGY

Besides the above mentioned compounds, seven other species of HAA (monobromoacetic acid (MBA), dichloroacetic acid (DCA), bromochloroacetic acid (BCA), bromodichloroacetic acid (BDCA), dibromoacetic acid (DBA) dibromochloroacetic acid (DBCA), and tribromoacetic acid (TBA)) are also included as target compounds because it could not be decided whether it is appropriate to choose the TDI approach at present time since the poor knowledge on their genotoxic potentials.

Two market-basket surveys were conducted in Kyoto, Japan from November 2007 to August 2009.

For each survey, 121 items of food were randomly purchased to represent the 17 groups of typical dietary classification (Table 2). Among the 17 groups, ten of them were prepared through boiling or dissolving with local tap water and reagent water as the cooking matrix in the same manner.

Table 2. Dietary classification

Group	Preparation	Daily intake (kg)
Grain	Boiling (30 min for rice and 10 min for others)	0.45
Potato	Boiling (10 min)	0.06
Sweetener	Dissolving in cold water	0.01
Bean	Boiling (10 min)	0.06
Nut	None	0.00
Vegetable	Boiling (5 min)	0.25
Fruit	None	0.12
Mushroom	Boiling (5 min)	0.02
Algae	Reconstituting in cold water (5 min)	0.01
Seafood	None	0.08
Meat	Fry (10 min)	0.08
Egg	None	0.03
dairy	None	0.14
Lipid	None	0.01
Snack	None	0.03
Beverage	Dissolving and extracting in hot water	0.62
Seasoning	Dissolving in cold water	0.09

Immediately after preparation, food samples were homogenized with a food processor and blended according to their intake proportion in each group. Pasted samples were stored at -20 °C and analysed within 48 hours. The extraction procedures were developed based on literature method (Tamakawa *et.al.*, 1987 and Raymer *et al.*, 2000) as follow.

THMs

(a) Disperse 100-g dietary sample in 200 mL of reagent water containing several boiling stones and approximately 0.15 mL of silicone antifoam.
(b) Add 10 mL of phosphoric aqueous solution (10%), 10 mL of sodium sulfite aqueous solution (10%) and 10 mL of n-hexane.
(c) Add 10 mL of phosphoric aqueous solution (10%), 10 mL of sodium sulfite aqueous solution (10%) and 10 mL of n-hexane.
(d) Extract THMs using a Dean-Stark distillatory apparatus. Cooling water was provided with a Yamato (Tokyo, Japan) CF-300 reflux condenser. The apparatus collects water and organic solvent that contains THMs from the mixture solution, and they separate into two phases.
(e) After 60-minute of distillation, take 4 mL of n-hexane layer out and allow it to cool for 5 minutes.
(f) Add 1 mL hexane with p-bromofluorobezene (10 mg/L) to the extract just prior to analysis.
(g) Transfer 2 mL of the sample to a sampler-vial and analyze it using a Shimadzu (Kyoto, Japan) GC-14B gas chromatograph equipped with electron-capture detector (63 Ni) (Table 3).

HAAs

(a) Disperse 2-g dietary sample in 10 mL of reagent water and homogenize it.
(b) Add 3 mL of 0.5 M phosphate buffer at pH 6.2. Check the pH of the solution using narrow range pH indicator strips. Add more buffer if the pH is less than 6.2.
(c) Adding 20 mL of MTBE and shaking for 15 minutes to remove the potentially interfering compounds. After centrifugation, remove the separated organic layer.
(d) Adjust the pH to near zero using 0.5 mL of concentrated sulfuric acid.
(e) Add 3 g of anhydrous sodium sulfate and 0.5 g of copper sulfate pentahydrate and shake immediately until almost all of them are dissolved.
(f) Add 4 mL of MTBE with 1, 2, 3-trichloropropane as an internal standard and shake the sample for 15 minutes.
(g) After centrifugation, take out 3 mL of the MTBE layer to a conical 15-mL centrifuge tube and add 3 mL of 10% sulfuric acid in methanol.
(h) Cap and vortex the tube, and incubate it in a heating block at 50 °C for 120 minutes to form methyl esters of HAAs.
(i) Cool the sample for 10 minutes and add 7 mL of sodium sulfate aqueous solution (150 g/L).
(j) Adjust the sample pH to neutral with 1 mL of saturated sodium bicarbonate aqueous solution with frequent ventilation.
(h) Transfer 2 mL of the MTBE layer to sampler-vial. A Shimadzu (Kyoto, Japan) QP2010 Plus gas chromatograph equipped with mass spectrometry was used for the quantification (Table 3).

Table 3. Analytical conditions

	THMs	HAAs
Column	J & W DB-624 (0.53 mm×30 m, film 3.0 μm)	J & W DB-5 (0.32 mm×30 m, film 0.25 μm)
Program of GC oven	50 °C (6 min) - 2 °C/min - 78 °C - 20 °C - 220 °C (15 min)	40 °C (6 min) - 2.5 °C/min - 65 °C - 20 °C - 205 °C (5 min)
Injection	200 °C, splitless	230 °C, splitless
Detection	280 °C	200 °C
Purge gas	Nitrogen (25 mL/min)	-
Carrier gas	Helium (8 mL/min)	Helium (2.04 mL/min)

The tap water and reagent water used as cooking matrix were also analyzed by the similar procedures. The extraction recoveries from dietary were investigated through the entire extraction procedure by introducing appropriate mass of analytes dissolved in hexane (THMs) and MTBE (HAAs) to 100 g and 2 g dietary sample respectively, and conducting the entire extraction procedure. The measured analyte concentrations were corrected with their determined recoveries. Method Quantification Limit (MQL) was defined as the THM concentrations that give the signal-to-noise ratios of 10. Concentrations below the MQL were expressed as None Detected (ND), and calculated as zero in the following exposure assessment.

Exposure Assessment

Situation (a)

Daily ingestion exposure via tap water intake (μg)
= tap water concentration (μg/L) × daily water consumption (L) Eq. (2)

Daily ingestion exposure via dietary (μg)
$= \sum$ (Tap-water-prepared dietary concentration (μg/kg) × daily dietary consumption (kg) Eq. (3)

The 2-Litre daily water consumption was applied in this evaluation. And daily dietary consumptions were based on the literature values (National Institute of Health and Nutrition, 2006). ND values were calculated as zero in the exposure assessment.

Situation (b)

Daily ingestion exposure via direct tap water intake (μg)
= tap water concentration (μg/L) × daily direct tap water consumption (L) Eq. (4)

Daily ingestion exposure via indirect tap water intake (μg)
= Daily ingestion expsoure via tap-water-prepared dietary (μg) - daily ingestion exposure via reagent-water-prepared dietary (μg) Eq. (5)

Daily ingestion exposure via dietary (μg)
$= \sum$ (Reagent-water-prepared dietary concentration (μg) × daily dietary consumption (kg) Eq. (6)

For daily direct tap water consumption, Mons *et al.* (2007) recommend using a 3.49 glasses of water/day (349 - 523 mL/day with a consumption of 100 mL to 150 mL glass volumes) as a conservative estimation for quantitative microbiological risk assessment. Yano *et al.* (2000) estimated the arithmetic mean value of direct tap water intake was 0.21 mL/day. This value was applied here because it was based on a domestic investigation. And daily dietary consumptions of foods or beverages were the same as explained in situation (a).
Inhalation and transdermal exposure were cited from previous research results for both situations (Quan *et al.*, 2007 and Itoh *et al.*, 2008).

RESULTS AND DISCUSSIONS

THM and HAA ingestion exposure via tap water intake

Based on the compound concentrations in reagent water and tap water as cooking matrixes, THM and HAA ingestion exposure via tap water intake are shown in Table 4.

THM and HAA Concentrations in Dietary Samples

TCM was found from samples without preparation and those prepared with tap water in a range from 0.02 to 32 ng/g (Table 5). The algae group had the highest concentration of TCM (32 ng/g), followed by the seasoning (18.9 ng/g), meat (12.8 ng/g) and sweetener groups (10.2 ng/g). Among these four groups, three of them were prepared with cold tap water. This is probably because the volatilization of TCM did not occur under lower temperature. BDCM and DBCM were detected from almost all the samples. TBM was not detected from all samples. DCA and TCA were most frequently detected, followed by MBA and MCA. Others were not detected from all or most of the dietary samples except from a few specific items such as seafood (DBA, 9.29 ng/g), nut (BCA, 13.3 ng/g), and algae (DBCA, 7.9 ng/g). Comparing with THMs, HAAs were not generally contained in the dietary, but could be found in specific items. Table 5 also shows that TCM, BDCM and DBCM were detected from the dietary prepared with reagent water in lower range compared to the samples prepared with tap water. TCM, BDCM, and DBCM concentrations were higher in every dietary

group prepared with tap water than its corresponding sample prepared with reagent water. Same observation could be also found in HAAs. These observations imply that preparing food with tap water led some samples to higher contamination levels of THMs and HAAs.

Table 4. THM and HAA ingestion exposure via direct tap water intake (μg/day)

	TCM		BDCM		DBCM	
	Situation (a)	Situation (b)	Situation (a)	Situation (b)	Situation (a)	Situation (b)
Tap water	19.0	1.99	10.7	1.12	5.70	0.60
Reagent water	0	0	0	0	0	0

	MCA		MBA		DCA		TCA	
	Situation (a)	Situation (b)	Situation (a)	Situation (b)	Situation (a)	Situation (b)	Situation (a)	Situation (b)
Tap water	0	0	0	0	9.90	1.04	12.0	1.26
Reagent water	0	0	0	0	0	0	0	0

	BCA		DBA		DBCA	
	Situation (a)	Situation (b)	Situation (a)	Situation (b)	Situation (a)	Situation (b)
Tap water	8.28	0.87	0	0	0.14	0.01
Reagent water	0	0	0	0	0	0

THM and HAA Ingestion Exposure via Dietary

It was found that the daily dietary intake amount was the main factor governing the ingestion exposure amount. Although the highest TCM concentration was detected in algae group, its exposure amount was 0.41 μg/day due to its small daily intake amount. On the contrary, the much larger daily intake of beverage group led to nearly 15 times higher exposure amount (6.11 μg/day) than that of algae. For both BDCM and DBCM, the greatest contributor among dietary samples was also beverage. The estimated TCM, BDCM and DBCM total ingestion exposure via dietary were 12.3, 2.64 and 1.15 μg/day. In HAAs, the exposure amount of TCA was the highest (22.9 μg/day), followed by DCA (20.8 μg/day). Tables 5 shows that TCM ingestion exposure via dietaries prepared with tap water was much higher than those with reagent water. For BDCM and DBCM, the differences were even greater than TCM. And in HAAs, DCA and TCA ingestion exposure amounts via tap-water-prepared dietaries were approximately as three times and twice high as those of reagent water. Similar observation could also be found in DBA. No great difference was observed for MCA and MBA. However, in the case of BCA and DBCA, exposure amount via reagent-water-prepared dietaries was higher than that of tap water. This is because higher concentrations were detected from reagent-water-prepared potato group (BCA) and bean group (DBCA). Needham (1999) found losses of BCA and DBCA in boiled water samples due to decomposition. It is possible that in different matrixes (such as reagent solution and more complicated tap water solution) the decarboxylation is taking place in different speed. Further study should be conducted on this point, but the two compounds were excluded from further estimation in this research. Generally, those observations indicate that preparing food with tap water does influence the THM and HAA ingestion exposure. Although applying the ingestion exposure via dietary prepared with tap water to the exposure assessment reflects the real-life exposure scenario, but it is not precise enough to estimate the allocation factor.

Table 5. THM and HAA concentrations and exposure amounts in (via) dietaries [a]

Preparation	TCM		BDCM		DBCM	
	Concentration (μg/kg)	Exposure (μg/day)	Concentration (μg/kg)	Exposure (μg/day)	Concentration (μg/kg)	Exposure (μg/day)
Tap water	0.02-32	12.3	ND-6.45	2.64	ND-3.39	1.15
Reagent water	ND[b]-18.7	4.22	ND-0.48	0.84	ND-0.3	0.44

Preparation	MCA		MBA		DCA		TCA	
	Concentration (μg/kg)	Exposure (μg/day)	Concentration (μg/kg)	Exposure (μg/day)	Concentration (μg/kg)	Exposure (μg/day)	Concentration (μg/kg)	Exposure (μg/day)
Tap water	ND-4.37	0.66	ND-89.6	1.67	ND-20.2	20.8	ND-37.1	22.9
Reagent water	ND-4.1	0.63	ND-39.9	1.38	ND-10.1	7.25	ND-24.6	11.8

Preparation	BCA		DBA		DBCA	
	Concentration (μg/kg)	Exposure (μg/day)	Concentration (μg/kg)	Exposure (μg/day)	Concentration (μg/kg)	Exposure (μg/day)
Tap water	ND-13.3	0.03	ND-9.29	0.77	ND-7.9	0.1
Reagent water	ND-4.0	0.27	ND	0	ND-14.9	0.92

[a] TBM, BDCA and TBA were excluded because they were not detected in any samples.

[b] Not detected

Allocation factors of THMs and HAAs

The allocation factors were preliminarily calculated as shown in Table 6. Except for MCA, MBA and DBA, all the allocation factors were estimated to be higher than the currently default value (20%). This implies that the current standard value derivation stands on the safe side of allocation factor. For THMs, the estimated allocation factors under situation (b) were numerically smaller than (a). And for MCA, MBA and DBA, it could be observed that in situation (a), since the ingestion exposure via indirect tap water intake was ignored, the factors could not be derived. However, after separately consider the direct and indirect tap water intake, the allocation factors for the three compounds are estimated in a more rational way. And in case of DCA and TCA, the allocation factors are estimated to be higher than situation (a).

Table 6. Allocation factors of THMs and HAAs

	Situation (a)	Situation (b)
TCM	0.47	0.43
BDCM	0.51	0.26
DBCM	0.54	0.24
MCA	0.00	0.05
MBA	0.00	0.17
DCA	0.32	0.66
TCA	0.34	0.51
DBA	0.0	0.97

CONCLUSIONS

(a) Preparing food with tap water led dietaries to higher contamination levels of THMs and HAAs, and also higher ingestion exposure in general.
(b) It is necessary to consider the ingestion exposure via direct and indirect tap water intake (as cooking matrix) separately, when estimate the allocation factors of THMs and HAAs.

REFERENCES

Clark, R. M., Goodrich, J.: Drinking water and cancer mortality, *Sci. Total Environ.*, Vol. 53, pp. 153-72, 1992.

Itoh, S., Quan, D., Muto, T., Okashita, R., Echigo, S., and Ohkouchi, Y.: Multiroute Exposure Assessment to Haloacetic Acids, (in Japanese), *Environ. Eng. Res*, Vol. 45, pp. 547-561, 2008.

Ministry of Health, Labor and Welfare, Japan: The national health and nutrition survey in Japan, (in Japanese), 2006.

Ministry of Health, Labor and Welfare, Japan: The revision of drinking water quality standard, (in Japanese), 2009.

Mons, M. N., van der Wielen, J. M. L., Blokker, E. J. M., Sinclair, M. I., Hulshof, K. F. A. M., Dangendorf, F., Hunterd, P. R., and Medema, G. J. : Estimation of the consumption of cold tap water for microbiological risk assessment: an overview of studies and statistical analysis of data, *J. Water Health*, Vol.5, pp. 151-170, 2007.

Needham, L. L.: Analytical challenges for assessing environmental exposure to children, symposia papers presented before the division of environmental chemistry, American Chemistry Society, Vol.39, pp.127-128, 1999.

Quan, D., Muto, T., Yanagibashi, Y., Itoh, S., Echigo, S., Ohkouchi, Y., Jinno, H.: Exposure assessment of trihalomethanes in households for estimating allocation to drinking water, Advances in *Asian Environ. Eng.*, Vol.6, pp.43-48, 2007.

Raymer, J.H., Pellizzari, E.D., Childs, B., Briggs, K., and Shoemaker, J.A.: Analytical methods for water disinfection byproducts in foods and beverages. *JESEE*, Vol.10, pp.808-815, 2000.

Tamakawa, K., Mishima, Y., Seki, T., and Tsunoda, A. : Determination of minute Quantities of Chloroform in Foods, (in Japanese), *Drinking Water and Food on the Citizens of Sendai,* Vol. 27, pp. 245-251, 1985.

Yano, K., Hosaka, M., Otaki, M., Tanaka, A., Iyo, T., Tosa, K., and Ichikawa, H. : A questionnaire study on the water consumption, (in Japanese), *Proceeding of 3rd Symposium of Japan Society on Water Environment*, pp. 159-160, 2000.

WATER RESEARCH 45 (2011) 761–767

Available at www.sciencedirect.com

ScienceDirect

journal homepage: www.elsevier.com/locate/watres

Direct observation of solid-phase adsorbate concentration profile in powdered activated carbon particle to elucidate mechanism of high adsorption capacity on super-powdered activated carbon

*Naoya Ando, Yoshihiko Matsui, Taku Matsushita, Koichi Ohno**

Graduate School of Engineering, Hokkaido University, N13W8, Sapporo 060-8628, Japan

ARTICLE INFO

Article history:
Received 14 March 2010
Received in revised form
27 August 2010
Accepted 30 August 2010
Available online 6 September 2010

Keywords:
SPAC
FIB
SEM
EDXS
Isotherm
PSS
NOM

ABSTRACT

Decreasing the particle size of powdered activated carbon (PAC) by pulverization increases its adsorption capacities for natural organic matter (NOM) and polystyrene sulfonate (PSS, which is used as a model adsorbate). A shell adsorption mechanism in which NOM and PSS molecules do not completely penetrate the adsorbent particle and instead preferentially adsorb near the outer surface of the particle has been proposed as an explanation for this adsorption capacity increase. In this report, we present direct evidence to support the shell adsorption mechanism. PAC particles containing adsorbed PSS were sectioned with a focused ion beam, and the solid-phase PSS concentration profiles of the particle cross-sections were directly observed by means of field emission–scanning electron microscopy/energy-dispersive X-ray spectrometry (FE-SEM/EDXS). X-ray emission from sulfur, an index of PSS concentration, was higher in the shell region than in the inner region of the particles. The X-ray emission profile observed by EDXS did not agree completely with the solid-phase PSS concentration profile predicted by shell adsorption model analysis of the PSS isotherm data, but the observed and predicted profiles were not inconsistent when the analytical errors were considered. These EDXS results provide the first direct evidence that PSS is adsorbed mainly in the vicinity of the external surface of the PAC particles, and thus the results support the proposition that the increase in NOM and PSS adsorption capacity with decreasing particle size is due to the increase in external surface area on which the molecules can be adsorbed.

1. Introduction

Powdered activated carbon (PAC) is used for the treatment of drinking water because this versatile adsorbent removes a broad range of organic pollutants, including pesticides and other organic chemicals, taste and odor compounds, cyanobacterial toxins, and total organic carbon (Suffet and McGuire, 1980; World Health Organization, 2006). Although activated carbon is widely used, it is expensive, and the higher the grade and quality of the activated carbon, the greater its cost (Babel and Kurniawan, 2003). While attention has been focused on investigation of various replacements for activated carbon, enhancing its adsorption has also been studied. For example, reducing the particle size of activated carbon increases the rate of adsorbate uptake and thereby reduces the amount of activated carbon required (Randtke and Snoeyink, 1983; Najm

* *Corresponding author.* Tel./fax: +81 11 706 7280.
E-mail address: matsui@eng.hokudai.ac.jp (K. Ohno).
0043-1354/$ – see front matter © 2010 Elsevier Ltd. All rights reserved.
doi:10.1016/j.watres.2010.08.050

et al., 1990; Jia et al., 2005; Matsui et al., 2005, 2009,); therefore, pulverizing activated carbon has been used as a strategy for cost reduction. Although decreasing the particle size increases the adsorption rate, it has been long assumed that the adsorption capacity does not change with particle size (Randtke and Snoeyink, 1983; Najm et al., 1990). However, several studies have shown that activated carbon with a small particle size (e.g., 100/200 US sieve size, Weber et al., 1983; and 0.73 μm median diameter, Ando et al., 2010) has a higher adsorption capacity for NOM. This NOM adsorption capacity increase is explained by means of a mechanism whereby NOM is adsorbed more in the shell region close to the external surface of the particles than in the region inside the particles because NOM forms aggregates in activated carbon pores and does not fully penetrate the carbon particle (Ando et al., 2010), and a shell adsorption model (SAM) based on this mechanism is proposed and verified by means of adsorption isotherm data (Matsui et al., submitted for publication).

The radial profile of adsorbate concentration throughout a particle, however, has not been confirmed by direct observation. Generally, activated carbon adsorption data is interpreted on the basis of measurement of the adsorbate concentration in the bulk water phase, and the solid-phase concentration profile inside activated carbon particles has rarely been observed. Ahn et al. (2005) recently used microprobe laser-desorption laser-ionization mass spectroscopy to spatially resolve the intraparticle concentration profile within several granular adsorbents, including granular activated carbon particles (40 μm). The study demonstrated the complexity of the intraparticle diffusion process.

The objective of the current study was to directly observe the solid-phase adsorbate concentration profiles of PAC particles and thus verify the shell adsorption mechanism. PAC particles containing PSS as a model adsorbate were sectioned with a focused ion beam (FIB), and the intraparticle solid-phase concentration profiles were directly quantified at a 0.4-μm scale by means of energy-dispersive X-ray spectrometry (EDXS) in a field emission–scanning electron microscope (FE-SEM).

2. Materials and methods

2.1. *Adsorbents and adsorbate*

Commercially available PAC (Taikou-W, Futamura Chemical Industries Co., Gifu, Japan) was used as received (designated PAC-T) or pulverized in a bead mill (Metawater Co., Tokyo, Japan) to produce super-powdered activated carbon (SPAC) samples of various particle sizes, designated SPACa-T, SPACb-T, SPACc-T, and SPACd-T in order of increasing particle size. A slurry of each activated carbon sample was prepared in pure water and stored at 4 °C before use. The median particle diameters of the samples were 0.7 μm for SPACa-T, 1.1 μm for SPACb-T, 1.9 μm for SPACc-T, 3.0 μm for SPACd-T, and 11.8 μm for PAC-T (as determined with an LA-700 size distribution analyzer, Horiba, Kyoto, Japan). The sulfur content of PAC-T was determined by combustion (International Organization for Standardization, 1998; TOX-100, Mitsubishi Chemical Analytech Co., Mie, Japan) and ion chromatography (DX-120, Dionex Corp., California, USA). PSS (Polymer Standard Service, Mainz, Germany; Mw = 1100 Da; Mw/Mn < 1.2) was used as a model adsorbate (Matsui et al., submitted for publication).

2.2. *Preparation of PSS solutions and measurement of adsorption isotherms*

PSS solutions (initial concentrations, 4.7 and 104 mg/L) were prepared by dissolving PSS in sulfate-ion-free water containing $NaHCO_3$ (20 mg/L as alkalinity) and $CaCl_2$ (4.9 mg/L as Ca). The PSS solutions were adjusted to pH 7.0 ± 0.1 by the addition of HCl or NaOH as required, and the solutions were filtered through 0.2-μm PTFE (Polytetrafluoroethylene) membrane filters before being used for adsorption isotherm tests. The bottle-point technique was used to conduct the adsorption isotherm tests. Various amounts of activated carbon were added to the PSS solution with efficient mixing, and 125 mL aliquots from the solution containing PSS and activated carbon were transferred to 125 mL vials. The vials were then agitated on a shaker for 3 weeks. After the contents of the vials were filtered through a 0.2-μm PTFE membrane filter, the liquid-phase PSS concentrations were measured. The PSS concentrations were determined by UV absorption at a wavelength of 262 nm (UV-1700, Shimadzu Co., Kyoto, Japan) with a calibration line.

2.3. *Solid-phase PSS concentration profile in a PAC-T particle*

2.3.1. *Preparation of PAC-T samples*

To prepare PAC-T particles with adsorbed PSS (PSS-loaded PAC-T), we conducted batch adsorption in a 125 mL vial containing a suspension of PSS (103 mg/L), PAC-T (20 mg/L), $NaHCO_3$ (0.2 mmol/L), and $CaCl_2$ (0.12 mmol/L). Because the PAC concentration profiles were determined by means of EDXS analysis of the sulfur in PSS, no sulfate-ion was added. To prepare PAC-T particles without PSS (blank PAC-T), we conducted a blank test without PSS in a 125 mL vial containing a suspension of PAC-T (20 mg/L), $NaHCO_3$ (0.2 mmol/L), and $CaCl_2$ (0.12 mmol/L). After the vials were shaken for 3 weeks, the PAC-T particles were recovered from the vials by means of centrifugal separation (1000 rpm, 190 *g*, 10 min). The particles were dried for 24 h at about 40 °C.

2.3.2. *FIB sectioning of PAC-T particles*

PAC-T particles were placed on a silicon (Si) wafer that was mounted with double-stick carbon tape (Nisshin EM Co., Tokyo, Japan) on the specimen holder of the FIB system (FB-2100, Hitachi, Ltd., Tokyo, Japan). After desiccation at 40 °C, the sample surface was coated with a 20-nm layer of platinum (Pt) to avoid charge-up effects by means of ion sputtering equipment (JEC-1600, JEOL, Ltd., Tokyo, Japan). A PAC-T particle was selected arbitrarily during real-time scanning-ion microscope imaging, and tungsten (W) was FIB-deposited on the particle for 20 min to prevent damage to the PAC-T particle during FIB milling, which was performed at a beam energy of 40 kV (Fig. 1a). Deep trenches were grooved around the PAC-T particle by means of gallium (Ga) FIB milling such that a small cubic portion (micro-sample) of the Si wafer with the PAC-T particle on top remained; a corner of the small cubic portion (micro-bridge) was left to connect the micro-sample to the Si

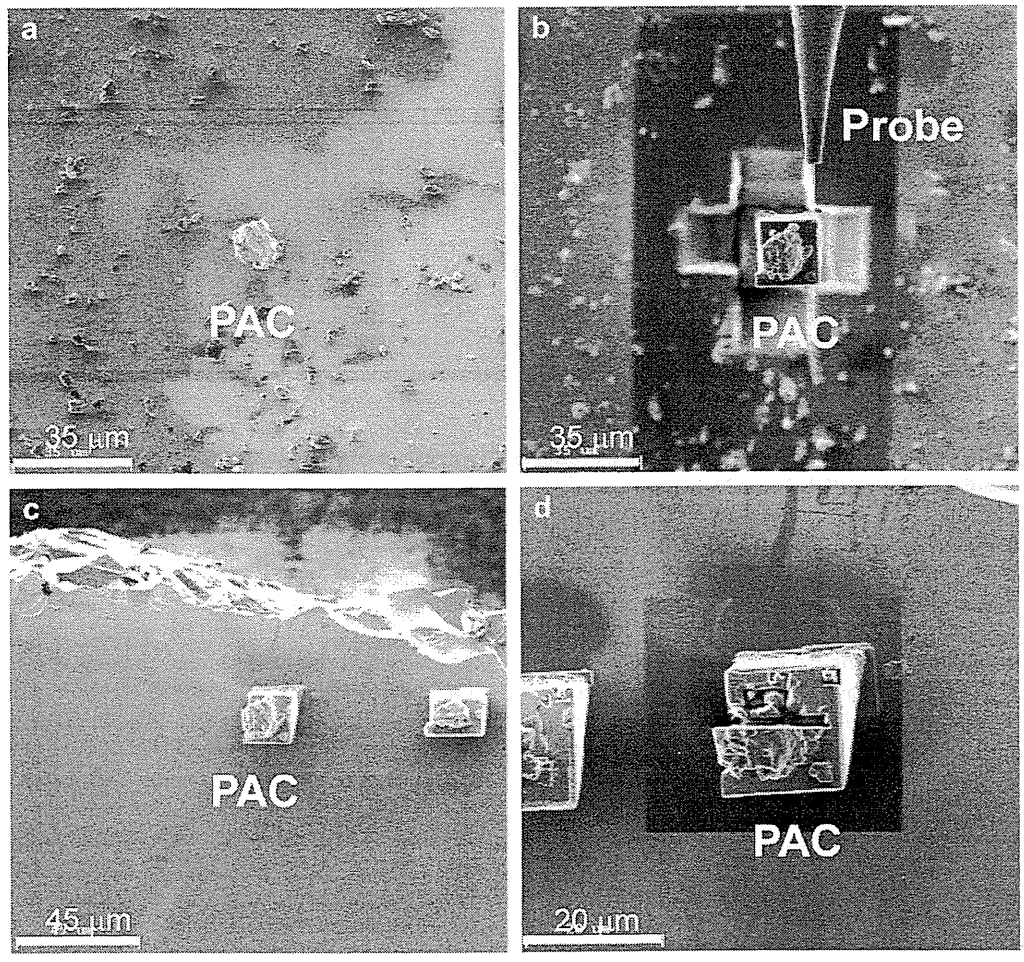

Fig. 1 – Micro-sampling and sectioning of a PAC-T particle using FIB: (a) PAC particles on silicon wafer; (b) micro-sample (small cube with a PAC particle on top) and a tungsten probe; (c) micro-samples on Si wafer, and (d) cross-section of PAC particle.

wafer. Subsequently, the specimen holder was tilted to 60°, and the bottom of the micro-sample was cut with a Ga FIB; as a result, the micro-sample was supported by a micro-bridge at one corner. A mechanical probe was inserted, and the tip of the probe was welded to the micro-sample by means of FIB-assisted W deposition (Fig. 1b). After the micro-bridge was cut with a Ga FIB, the micro-sample was separated from the Si wafer and placed on a newly inserted Si wafer by means of W deposition (4 min). The mechanical probe was cut with a Ga FIB (Fig. 1c) after the newly inserted wafer was mounted on the sample holder of the FIB system by double-stick carbon tape. About half of the PAC-T particle on the micro-sample was then cut away with a Ga FIB to leave a cut PAC-T particle (Fig. 1d). The cut particle was coated with a 2 nm layer of Pt by ion sputtering to avoid charge-up effects during SEM.

2.3.3. *FE-SEM/EDXS of a PAC-T particle*

The Si wafer with the FIB-cut PAC-T particle was mounted with double-stick carbon tape on an L-shaped holder (JEOL) for FE-SEM (JSM-7400F, JEOL) observation of the cross-section of the particle. EDXS line-scan chemical analysis was performed in 0.047-μm increments on the surface of the cross-sectioned particle in the FE-SEM (acceleration voltage, 10 kV; number of sweeps, 25; dwelling time, 0.1 s; magnification, 10,000; working distance, 8.0 mm; JED-2300, JEOL). The penetration depth of electron for the EDXS analysis could be considered large (Castaing, 1960). Lee et al. (2006)

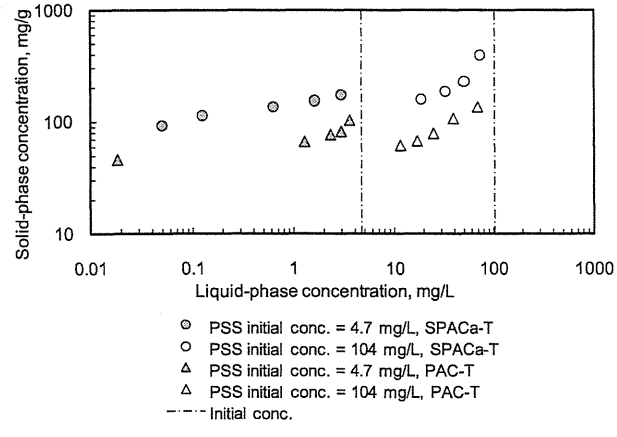

Fig. 2 – Adsorption isotherms of PSS.

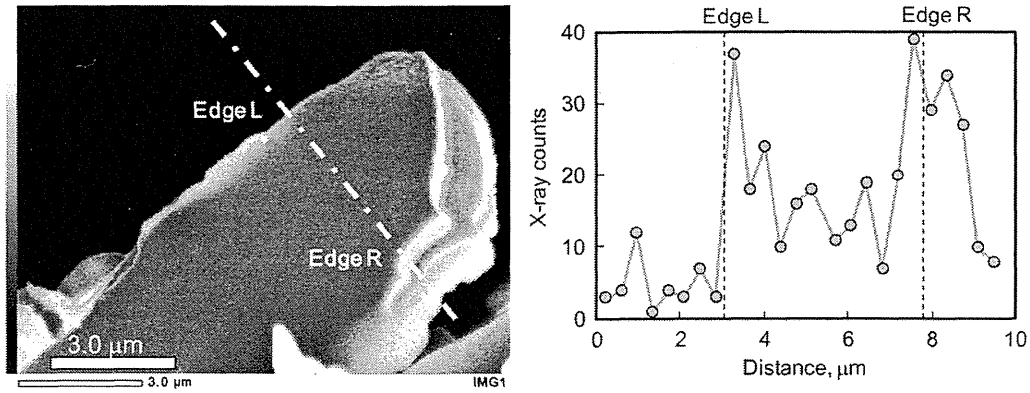

Fig. 3 – Left panel: SEM image of the cut face of a PSS-loaded PAC-T particle. EDXS line-scan analysis was conducted along the broken line in 0.047-μm increments. Right panel: Profile of X-ray counts from S obtained by EDXS line-scan analysis. The dashed lines indicate the particle boundaries.

estimate the penetration depth of 1.2 μm using 10-kV acceleration voltage for bulk carbon. Therefore, the EDXS would be regarded as center-weighted average metering scheme in the circle of around 0.6 μm radius if the penetration depth of 1.2 μm and the spherical penetration region were assumed and the diameter of the spherical penetration region was assumed to be equal to the penetration depth.

3. Results and discussion

3.1. *Adsorption isotherms and solid-phase concentration profile*

Our goal was to verify the hypothesis that organic macromolecules are adsorbed mainly on the shell region close to the external surface of powdered activated carbon particles and not in the inner region. Because the specific outer surface area (surface area per unit mass) available for adsorption is greater for smaller particles than for larger particles, this hypothesis would explain why the adsorption capacity of SPAC is larger than that of PAC. To verify the hypothesis, we used PSS as a model adsorbate and directly observed the cross-sectional profile of the PSS concentration in PAC-T particles by FE-SEM/EDXS. In previous work (Ando et al., 2010; Matsui et al., submitted for publication), in which we observed that the adsorption capacity of SPAC was larger than that of PAC, we used a PSS solution with a natural ion composition (including sulfate-ion). In contrast, in this study, we observed the PSS concentration profiles of PAC-T particles with adsorbed PSS in sulfate-ion-free water. Therefore, we first confirmed that in sulfate-ion-free water, the amount of PSS adsorbed on the SPAC was higher than that adsorbed on PAC-T (Fig. 2). Fig. 2 also suggests that a higher initial liquid-phase concentration lead to a lower solid-phase concentration. The reason for this phenomenon is not known, but this might be due to the slight heterogeneity of the PSS (Matsui et al., submitted for publication): for heterogeneous adsorbate, the isotherm results depend on the initial concentration (Sontheimer et al., 1988).

Because the sulfur (S) in PSS is in a sulfonic acid group and activated carbon contains little S (0.28 mg-S/g), the characteristic X-ray emissions from S (Kα, 2.307 keV; He et al., 1999) were counted as a measure of PSS concentration. The X-ray emission counts were scanned in 0.047 μm increments along the FIB-cut surface of a PSS-loaded PAC-T particle (Fig. 3, left

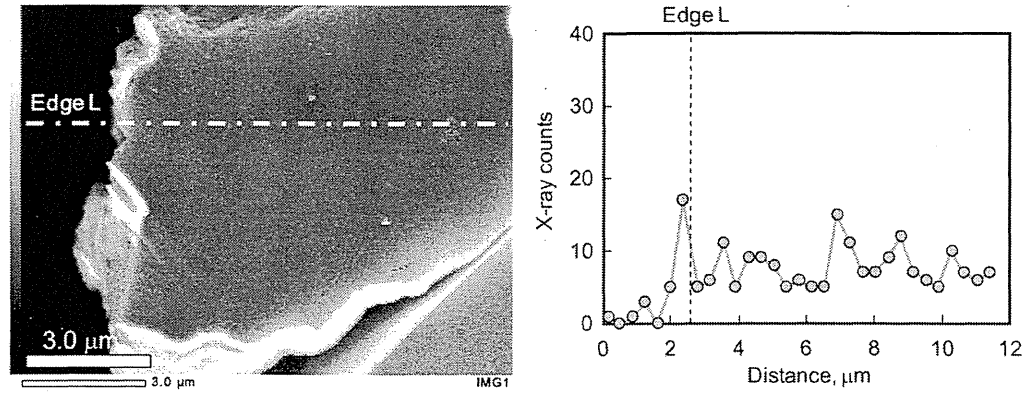

Fig. 4 – Left panel: SEM image of the cut face of a blank PAC-T particle. EDXS line-scan analysis was conducted along the broken line crossing. Right panel: Profile of X-ray counts from S obtained by EDXS line-scan analysis. The dashed line indicates the particle boundary.

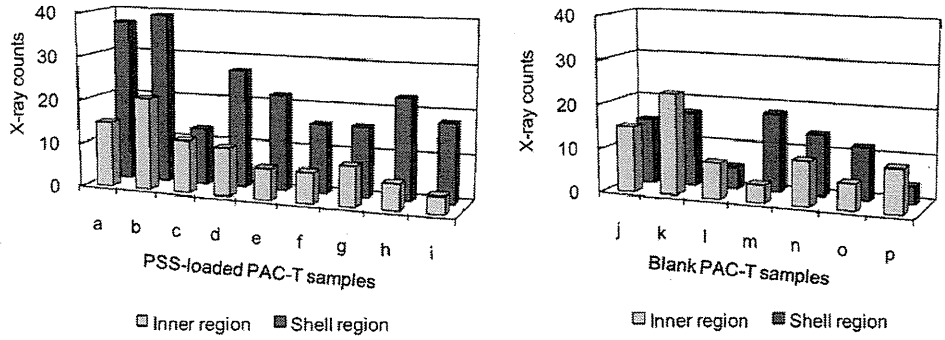

Fig. 5 – Comparison of X-ray counts in the shell and inner regions of PAC-T particles. Left panel: X-ray counts for PSS-loaded PAC-T particles a–i. Right panel: X-ray counts for blank PAC-T particles j–p. X-ray counts obtained from 0.024 to 0.400 μm (0.376-μm range) from the outer surface were summed as the counts for the shell region, and the counts obtained from 2.024 to 2.400 μm (0.376-μm range) from the interface were summed as the counts for the inner region.

panel, broken line). The characteristic X-ray emission from S was weak because X-ray production is inherently low for light elements such as S and because the amount of PSS adsorbed on the PAC-T was small (63 mg-S/g) relative to the amount of carbon. Therefore, the X-ray emission counts obtained for each 0.047-μm increment were small, and the counts were summed for each 0.376-μm interval and are plotted in Fig. 3 (right panel). The data showed some scatter, but the X-ray counts for S were clearly higher in the region close to the outer surface of the particle than in the inner region. High X-ray counts were also observed beyond the external surface of the particle (beyond Edge R in Fig. 3), but these high counts may have been due to high PSS loading on the external particle surface or to irregular X-ray scattering arising from surface roughness, which can be seen in the SEM image. The X-ray emission profile for a blank PAC-T particle did not show higher X-ray emission counts outside the particle relative to the counts inside; the emission count profile was roughly flat for the blank PAC-T particle (Fig. 4).

3.2. *Statistical hypothesis testing*

Although the FE-SEM/EDXS results (Figs. 3 and 4) supported the SAM, analytical errors were associated with the data. To verify the SAM, we prepared additional PSS-loaded PAC-T and blank PAC-T particles, cut the particles with the FIB, conducted EDXS line-scan analyses, and measured X-ray counts for the shell regions (0.024–0.400 μm from the outer surface) and the inner regions (2.024–2.400 μm from the outer surface).

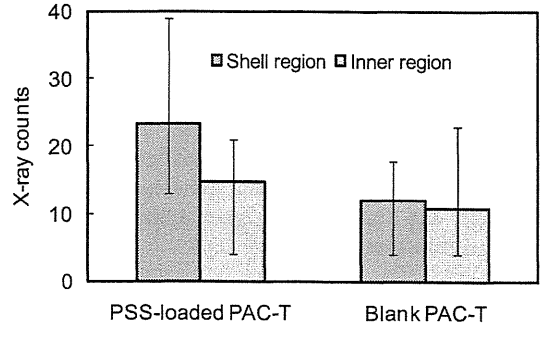

Fig. 6 – Mean X-ray counts in shell and inner regions of PSS-loaded PAC-T (n = 9) and blank PAC-T (n = 7) particles. Error bars indicate maximum and minimum values.

Comparison of the X-ray counts for the shell region and the inner region of each PSS-loaded PAC-T particle (Fig. 5, left panel) indicated that the X-ray counts for each particle were always higher in the shell region than in the inner region. For the blank particles, the X-ray counts in the shell region were not consistently higher or lower than the counts in the inner region (Fig. 5, right panel). Note that for the PSS-loaded PAC samples, the X-ray counts in the shell regions of some of the particles were lower than the counts in the inner region of other particles: for example, the X-ray counts in the shell region for PSS-loaded PAC particle "c" were lower than the X-ray counts in the inner region for PSS-loaded PAC particle "a"; that is, the ranges for the shell region and the inner region overlapped each other (Fig. 6). Therefore, we cannot definitively say that the X-ray counts in the shell region were higher than the counts in inner region. However, the overlap may have resulted from data scattering arising from the low sensitivity of S in EDXS.

To determine whether the difference between the X-ray counts in the shell region and the inner region was statistically significant, we conducted statistical hypothesis tests. The tests indicated that for PSS-loaded PAC-T, the mean number of X-ray counts in the shell region was 23.4, whereas the number of counts in the inner region was 10.2 (Fig. 6). For blank PAC-T particles, in contrast, the mean number of X-ray counts in the shell region was 12.1, whereas the number of counts in the inner region was 10.9. The statistical significance of the difference between the two mean counts was evaluated by means of the equal-variance Student's T-test after the homogeneity of variances was tested by means of the F-test. For PSS-loaded PAC-T, the P-value for the null hypothesis H_0 (that is, the hypothesis that there was no difference in the variance of counts between the shell and inner regions) was 12.9%, and the corresponding P-value for blank PAC-T particles was 75.1% (Table 1). Therefore, the null hypothesis could not be rejected for either PAC sample. By assuming the variances of counts were the same for the shell region and the inner region, we conducted the equal-variance

Table 1 – Results of F-test.

	PSS-loaded PAC-T		Blank PAC-T	
Variance of counts	Shell region	86.3	Outside	31.1
	Inner region	27.7	Inside	40.8
H_0: Null hypothesis	No difference in mean counts			
F-value	3.12		1.31	
P-value (%)	12.9		75.1	

Student's T-tests for the null hypothesis H_0 (that is, the hypothesis that there was no difference in the population means of counts between the shell and inner regions). The null hypothesis was rejected at the 0.2% level for the PSS-loaded PAC-T, whereas the null hypothesis could not be rejected for the blank PAC-T particles (P-value = 69.5%; Table 2). In summary, the statistical tests clearly indicated that the X-ray counts were different between the shell region and the inner region of PSS-loaded PAC-T particles, but for the blank PAC-T particles, the difference between the X-ray counts in the shell and inner regions was not statistically significant. Thus, we conclude that for the PSS-loaded PAC-T particles, the solid-phase concentration of PSS was higher on the outside than in the inside of the particles. Therefore, the results of the EDXS line-scan analysis clearly supported the hypothesis that the PSS was adsorbed mainly in the vicinity of the outer surface. Consequently, PAC particles, which have less outer surface area than SPAC particles, can be expected to show reduced adsorption capacity.

3.3. *Comparison with shell adsorption model*

The SAM assumes a pattern of adsorbate concentration profile described by two parameters: δ, which is the thickness of the shell (penetration depth), and *p*, which is a dimensionless parameter that defines availability of internal porous structures for adsorption. Once these parameter values are known, the solid-phase adsorbate concentration profile can be depicted. The determination of these parameter values requires the isotherm data for adsorbent particle of different sizes. In this study, the isotherm data for SPACb-T, SPACc-T and SPACd-T (Fig. 1S in the supplementary information) as well as SPACa-T and PAC-T (Fig. 2) were obtained with same PSS solution prepared for the analysis of the PAC-T samples by FE-SEM/EDXS, and the isotherm data were analyzed by means of the SAM (Matsui et al., submitted for publication). The PSS concentration profile in a PAC-T particle is depicted in Fig. 7 (solid line). The SAM results suggest that the shell was thin (shell thickness, 0.16 μm) and that the PSS load was high in the shell region. From the profile of the X-ray counts for S, however, we could not confirm the thinness of the shell, because of the low density of the data (as mentioned earlier, the X-ray emission counts were summed for each 0.376-μm interval). For comparison, we determined a moving-average PSS concentration profile for 0.376-μm intervals so that we could compare the results of the SAM analysis and the X-ray counts over the same data-acquisition interval. The moving-average PSS profile was similar to the characteristic X-ray profile, but because of data scattering and the small number of data points over the distance, we could not unequivocally conclude that the two profiles were consistent. If the two profiles were different, there are two possible explanations. First, PSS molecules may have diffused into the inner region during preparation of PAC-T samples and the FIB cutting process. Second, the effect of the large evolution area of the characteristic X-rays must be considered (Lee et al., 2006); the large area means that the EDXS method is center-weighted average metering scheme rather than spot metering scheme and the obtained X-ray counts were inevitably area-averaged counts (Castaing, 1960).

Table 2 – Results of student's T-test.

	PSS-loaded PAC-T		Blank PAC-T	
Mean counts	Shell region	23.4	Outside	12.1
	Inner region	10.2	Inside	10.9
H_0: Null hypothesis	No difference in mean counts			
Pooled variance	57.0		36.0	
T-value	3.72		0.40	
P-value (%)	0.2		69.5	

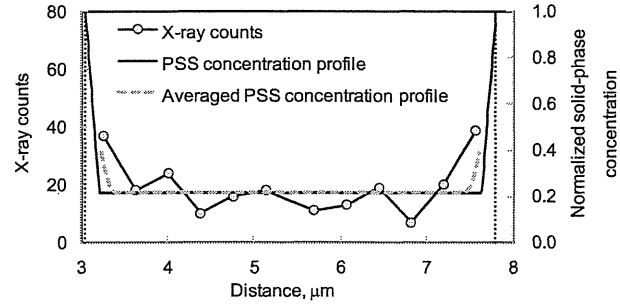

Fig. 7 – Comparison of characteristic X-ray profile (see Fig. 3) and PSS solid-phase concentration profiles. Circles: characteristic X-ray profile for S. Solid line: PSS solid-phase concentration profile obtained by SAM and PSS adsorption isotherm data. Dashed gray line: Moving-average profile of the PSS solid-phase concentration. Vertical dotted lines: Particle boundaries.

4. Conclusions

PSS-loaded and blank PACs were cut by FIB, and the solid-phase PSS concentration profiles of the particle cross-sections were directly observed by means of FE-SEM/EDXS line-scan analysis. PSS was adsorbed mainly in the shell region close to the outer surface of the particles and less so in the inner region. These results confirmed that the shell adsorption mechanism can explain the higher adsorption capacity of SPAC relative to that of PAC.

Acknowledgements

This study was supported by a Grant-in-Aid for Scientific Research A (21246083) from the Ministry of Education, Science,

Sports and Culture of the Government of Japan; a research grant from the Ministry of Health, Labor and Welfare; and by Metawater Co., Tokyo, Japan.

Appendix. Supplementary data

Supplementary data associated with this article can be found, in the online version, at doi:10.1016/j.watres.2010.08.050

REFERENCES

Ahn, S., Werner, D., Karanagioti, H.K., Mcglaothlin, D.R., Zare, R.N., Luthy, R.G., 2005. Phenanthrene and pyrene sorption and intraparticle diffusion in polyoxymethylene, coke, and activated carbon. Environmental Science and Technology 39 (17), 6516–6526.

Ando, N., Matsui, Y., Kurotobi, Y., Nakano, Y., Matsushita, T., Ohno, K., 2010. Comparison of natural organic matter adsorption capacities of super-powdered activated carbon. Water Research 44 (14), 4127–4136.

Babel, S., Kurniawan, T.A., 2003. Low-cost adsorbents for heavy metals uptake from contaminated water: a review. Journal of Hazardous and Materials 97 (1–3), 143–219.

Castaing, R., 1960. Electron probe microanalysis. Advances in Electronics and Electron Physics 13, 317–386.

He, A.J., Yang, K.V., Dolukhanyan, T., Sung, C., Kumar, J., Tripathy, K.S., Samuelson, L., Balogh, L., Tomalia, A.D., 1999. Electrostatic multilayer deposition of a gold-dendrimer nanocomposite. Chemistry of Materials 11 (11), 3268–3274.

International Organization for Standardization (ISO 11632:1998), 1998. Stationary Source Emissions–Determination of Mass Concentration of Sulfur Dioxide–Ion Chromatography Method. International Organization for Standardization, Geneva.

Jia, Y., Wang, R., Fane, A.G., Krantz, W.B., 2005. Effect of air bubbling on atrazine adsorption in water by powdered activated carbons–competitive adsorption of impurities. Separation and Purification Technology 46 (1–2), 79–87.

Lee, S., Younan, H., Siping, Z., Zhiqiang, M., 2006. Studies on electron penetration versus beam acceleration voltage in energy-dispersive X-ray microanalysis. Proc. ICSE 2006, IEEE International Conference, Kuala Lumpur, Malaysia, pp. 610–613.

Matsui, Y., Murase, R., Sanogawa, T., Aoki, N., Mima, S., Inoue, T., Matsushita, T., 2005. Rapid adsorption pretreatment with submicron powdered activated carbon particles before microfiltration. Water Science and Technology 51 (6–7), 249–256.

Matsui, Y., Ando, N., Sasaki, H., Matsushita, T., Ohno, K., 2009. Branched pore kinetic model analysis of geosmin adsorption on super-powdered activated carbon. Water Research 43 (12), 3095–3103.

Matsui, Y., Ando, N., Yoshida, T., Kurotobi, R., Matsushita, T., Ohno, K. Modeling high adsorption capacity and kinetics of organic macromolecules on super-powdered activated carbon. Water Research, submitted for publication.

Najm, I.N., Snoeyink, V.L., Suidan, M.T., Lee, C.H., Richard, Y., 1990. Effect of particle size and background natural organics on the adsorption efficiency of PAC. Journal of American Water Works Association 82 (1), 65–72.

Randtke, S.J., Snoeyink, V.L., 1983. Evaluating GAC adsorptive capacity. Journal of American Water Works Association 75 (8), 406–413.

Sontheimer, H., Crittenden, J.C., Summers, R.S., 1988. Activated Carbon for Water Treatment, second ed. DVGW-Forschungsstelle, Karlsruhe, Germany.

Suffet, I.H., McGuire, M.J., 1980. Activated Carbon Adsorption of Organics from the Aqueous Phase, vol. 1–2. Ann Arbor Science, Ann Arbor.

Weber, W.J.J., Voice, T.C., Jodellah, A., 1983. Adsorption of humic substances: the effects of heterogeneity and system characteristics. Journal of American Water Works Association 75 (12), 612–619.

World Health Organization, 2006. Guidelines for Drinking-Water Quality. third ed., vol. 1. recommendations, Word Health Organization, Geneva.

WATER RESEARCH 45 (2011) 1720–1728

Available at www.sciencedirect.com

ScienceDirect

journal homepage: www.elsevier.com/locate/watres

Modeling high adsorption capacity and kinetics of organic macromolecules on super-powdered activated carbon

Yoshihiko Matsui, Naoya Ando, Tomoaki Yoshida, Ryuji Kurotobi, Taku Matsushita, Koichi Ohno*

Graduate School of Engineering, Hokkaido University, N13W8, Sapporo 060-8628, Japan

ARTICLE INFO

Article history:
Received 3 March 2010
Received in revised form
15 November 2010
Accepted 15 November 2010
Available online 24 November 2010

Keywords:
Diffusion
Isotherm
Shell
Equilibrium
Homogeneous
surface diffusion
model (HSDM)

ABSTRACT

The capacity to adsorb natural organic matter (NOM) and polystyrene sulfonates (PSSs) on small particle-size activated carbon (super-powdered activated carbon, SPAC) is higher than that on larger particle-size activated carbon (powdered-activated carbon, PAC). Increased adsorption capacity is likely attributable to the larger external surface area because the NOM and PSS molecules do not completely penetrate the adsorbent particle; they preferentially adsorb near the outer surface of the particle. In this study, we propose a new isotherm equation, the Shell Adsorption Model (SAM), to explain the higher adsorption capacity on smaller adsorbent particles and to describe quantitatively adsorption isotherms of activated carbons of different particle sizes: PAC and SPAC. The SAM was verified with the experimental data of PSS adsorption kinetics as well as equilibrium. SAM successfully characterized PSS adsorption isotherm data for SPACs and PAC simultaneously with the same model parameters. When SAM was incorporated into an adsorption kinetic model, kinetic decay curves for PSSs adsorbing onto activated carbons of different particle sizes could be simultaneously described with a single kinetics parameter value. On the other hand, when SAM was not incorporated into such an adsorption kinetic model and instead isotherms were described by the Freundlich model, the kinetic decay curves were not well described. The success of the SAM further supports the adsorption mechanism of PSSs preferentially adsorbing near the outer surface of activated carbon particles.

1. Introduction

It has been thought that adsorption capacity of activated carbon does not depend on particle size because adsorption occurs in internal pores of activated carbon particles (Letterman et al., 1974; Najm et al., 1990; Peel and Benedek, 1980a and Leenheer, 2007); however, the effect of adsorbent particle size on adsorption capacity has not been examined sufficiently. With decreasing activated carbon particle size, the capacity to adsorb natural organic matter (NOM) has been reported both to not change (Randtke and Snoeyink, 1983) and to increase (Weber et al., 1983). Possible reasons for these contradictory results have been discussed, but a clear mechanism with supporting experimental evidence has not yet been presented.

Recently, very fine (median particle diameters of 0.7 μm) activated carbon particles (super-powdered activated carbon, SPAC) became available through advances in pulverization technology (Matsui et al., 2004, 2005, 2007, 2009a). Thus, it has become possible to reduce adsorbent particle diameter to the submicron range, which is ten times as small as the size of powdered-activated carbon (PAC). SPAC adsorbs NOM

* *Corresponding author.* Tel./fax: +81 11 706 7280.
E-mail address: matsui@eng.hokudai.ac.jp (Y. Matsui).
0043-1354/$ – see front matter © 2010 Elsevier Ltd. All rights reserved.
doi:10.1016/j.watres.2010.11.020

efficiently because of its high adsorption capacity as well as its kinetic properties. The high adsorption capacity of SPAC raises the issue of adsorption capacity dependence on adsorbent particle size. In the early stages of SPAC research, increased capacity for NOM adsorption on SPAC was thought to be attributable to the mesopore volume increase caused by the fracture of ink-bottle pore structures during pulverization (Matsui et al., 2004). However, it later became apparent that structural changes in pore size distribution attributable to pulverization were not large, and the capacity increase for NOM adsorption could not be explained adequately by an increase in mesopore volume. Instead, it has been proposed that the capacity increase for NOM adsorption on SPAC is due to adsorbate not penetrating completely into the adsorbent particle and preferentially adsorbing in the particle outer region close to the surface of the particle; we also proposed a conceptualization of this concept (Ando et al., 2010).

The objective of our current research is to verify and confirm this conceptualization through model analysis. To do so, we have developed adsorption isotherm and kinetic models based on the shell adsorption mechanism, and verified our findings with experimental data by using polystyrene sulfonates (PSSs) as model substances (Karanfil et al., 1996a,b; Li et al., 2003a,b; and Ando et al., 2010).

2. Materials and methods

2.1. Activated carbons

Commercially available PAC (Taikou-W, Futamura Chemical Industries Co., Ltd., Gifu, Japan) was used as received (PAC-T) or pulverized in a bead mill (Metawater Co., Ltd., Tokyo, Japan) to achieve four degrees of pulverization; we designated these super-powdered activated carbons as SPACa-T, SPACb-T, SPACc-T, and SPACd-T, in increasing order of particle size. The pore size distributions and the scanning electron micrographs of SPACa-T and PAC-T are presented elsewhere (Ando et al., 2010). Slurries of each activated carbon were prepared in pure water and stored at 4 °C and used after dilution and placement under vacuum. Particle size distributions of the five activated carbons were determined by using a laser-light scattering instrument (LA-700, Horiba, Ltd., Kyoto, Japan).

2.2. Water samples

PSSs with various molecular weights (MWs) were selected as model substances instead of NOM because PSSs are chemically homogeneous compounds with known MWs and narrow MW ranges, while NOM is a complex mixture of compounds with unknown composition. Thus, our selection of PSSs makes model analysis of adsorption equilibrium and kinetics clear and unambiguous. We refer to our first PSS formulation as PSS-4600 (Polysciences, Inc., Warrington PA, USA), with a weight-average MW (Mw) of 5180 Da and a number-average MW (Mn) of 4600 Da. Our second PSS formulation, referred to as PSS-1800 (Polysciences, Inc.), had an Mw of 1430 Da and an Mn of 1200 Da. Our final PSS formulation, referred to as PSS-1000 (Polymer Standard Service GmbH., Mainz, Germany), had an Mw of 1100 Da and an Mw/Mn of <1.2.

We dissolved the PSSs in ultrapure water after the addition of inorganic ions to adjust the ionic strength, and we adjusted the constituent inorganic ions and their concentrations to match those of natural water and the PSS waters used in previous experiments (Table 1S in the supplementary information, Matsui et al., 2004; Ando et al., 2010). All water samples were adjusted to pH 7.0 ± 0.1 by the addition of HCl or NaOH, as required; they were then filtered through 0.2-μm membrane filters (DISMIC-25HP, Toyo Roshi Kaisha, Ltd., Tokyo) before use in experiments. We determined PSS concentrations by UV absorption at a wavelength of 262 nm (UV-1700, Shimadzu Co., Kyoto, Japan).

2.3. Batch adsorption tests

We conducted PSS-1800 and PSS-1000 adsorption equilibrium tests with all five activated carbons, but we conducted PSS-4600 adsorption equilibrium tests only with SPACa-T, SPACd-T, and PAC-T. The experimental procedure, described in detail elsewhere (Ando et al., 2010), briefly is as follows. SPAC and PAC slurries were diluted, placed under vacuum, and added to 300-mL solutions containing adsorbate with mixing (Table 2S in the supplementary information). Aliquots (100 mL) were transferred from the 300-mL solutions to 125-mL vials, which were agitated on a shaker for 3 weeks at a constant temperature of 20 °C. Control tests were also conducted that did not contain carbon to confirm that concentration changes during long-term mixing were negligible. After filtering the water samples through a 0.2-μm membrane filter, we measured the liquid-phase adsorbate concentrations.

We investigated adsorption kinetics of SPACa-T, SPACd-T, and PAC-T by means of batch tests with efficient mixing. Sample water (3 L) containing PSSs was placed in a beaker, and an aliquot (50 mL) was withdrawn from the beaker to determine the initial PSS concentration. After the addition of a specified amount of an activated carbon suspension (Table 3S in the supplementary information), aliquots (50 mL) were withdrawn at intervals and filtered immediately through a 0.2-μm membrane filter for determination of PSS concentration.

3. Results and discussion

3.1. Shell adsorption model

Clearly adsorption capacity for PSS-4600, PSS-1800, and PSS-1000 on activated carbon (SPACa-T, SPACb-T, SPACc-T, SPACd-T, and PAC-T) increased with decreasing adsorbent particle size (Fig. 1 and Fig. 1S in the supplementary information). Adsorption sharply increased with increasing equilibrium concentration close to the initial concentration, in particular for PSS-1000. This could be due to the heterogeneity of PSS compounds (Karanfil et al., 1996a; Matsui et al., 1998), despite our assumption of homogeneity for the PSS compounds because of their small-MW ranges. Therefore, the data points for concentrations close to the initial concentration, indicated by red color in Fig. 1, were omitted from our mathematical analysis. Adsorption capacity for all three PSS formulations, as represented by q_{50}, increased with decreasing adsorbent particle size (Fig. 2). PSS adsorption